Skelton, A., Peillod, A., Glodny, J., Klonowska, I., Månbro, C., Lodin, K., Ring, U. (2019): Preservation of high-P rocks coupled to rock composition and the absence of metamorphic fluids. - *Journal of Metamorphic Geology*, *37*, 3, pp. 359—381.

DOI: http://doi.org/10.1111/jmg.12466

Title: **Preservation of high pressure rocks coupled to rock composition and the absence of metamorphic fluids**

Short running title: **Preservation of high pressure rocks**

Authors: Alasdair Skelton[1,*], Alexandre Peillod[1], Johannes Glodny[2], Iwona Klonowska[3], Carolina Månbro[1], Karin Lodin[1] and Uwe Ring[1]

Affiliations:

[1]*Department of Geological Sciences, Stockholm University, Stockholm, Sweden*

[2]*Deutsches GeoForschungsZentrum, GFZ, Telegrafenberg, Potsdam, Germany*

[3]*Department of Earth Sciences, Uppsala University, Uppsala, Sweden*

* Corresponding author: alasdair.skelton@geo.su.se

ABSTRACT

Eclogites, blueschists and greenschists are found in close proximity to one another along a 1-km coastal section where the Cyclades Blueschist Unit (CBU) is exposed on SE Syros, Greece. Here we show that the eclogites and blueschists experienced the same metamorphic history: prograde lawsonite blueschist facies metamorphism at 1.2–1.9 GPa and 410–530 °C followed, at 43–38 Ma, by peak blueschist/eclogite facies metamorphism at 1.5–2.1 GPa and 520–580 °C. We explain co-existence of eclogites and blueschists by compositional variation probably reflecting original compositional layering. We also show that the greenschists record retrogression at 0.34 ± 0.21 GPa and T = 456 ± 68 °C. This was spatially associated with a shear zone on a scales of 10-100-m and veins on a scale of 1-10-cm. Greenschist facies metamorphism ended at (or shortly after) 27 Ma. We thus infer a period of metamorphic quiescence after eclogite/blueschist facies metamorphism and before greenschist facies retrogression which lasted up to 11–16 million years. We suggest that this reflects an absence of metamorphic flow at that time and conclude that greenschist facies retrogression only

occurred when and where metamorphic fluids were present. From a tectonic perspective, our findings are consistent with studies showing that the CBU is 1) a high-pressure nappe stack consisting of belts in which high pressure metamorphism and exhumation occurred at different times and 2) affected by greenschist facies metamorphism during the Oligocene, prior to the onset of regional tectonic extension.

Keywords: HP-LT metamorphism; Metamorphic fluids; Bulk composition; Syros; Cyclades Blueschist Unit

1 | INTRODUCTION

Rocks metamorphosed at high pressure (HP) – low temperature (LT) conditions have fascinated petrologists for decades. This is at least partly because *HP-LT* rocks provide a record of tectonometamorphic processes in subduction zones. However, *HP-LT* mineral assemblages formed due to crustal thickening associated with subduction are often partly or entirely replaced at lower *P* and higher *T* conditions associated with exhumation (Ernst, 1988). Preservation of *HP-LT* rocks can reflect an absence of metamorphic fluids (Schiestedt & Matthews, 1987), restriction of fluid availability to specific *P-T* conditions (Schorn, 2018) or fluid composition effects (Breeding et al., 2003; Kleine et al., 2014). The presence or absence of metamorphic fluids as well as fluid composition effects, usually reflecting channelized fluid flow, provide possible explanations for the occurrence of *HP-LT* (eclogites and blueschists) rocks in close proximity to rocks that record metamorphism at lower *P* and/or higher *T* (greenschists, amphibolites and granulites) (Austrheim, 1987; Glodny et al., 2003, 2008a, 2008b; Jun & Klemd, 2000; Proyer, 2003; Young and Kylander-Clark, 2015).

Recent work suggests that in most cases, replacement of *HP-LT* mineral assemblages occurs in the parts of a rock volume that have come into contact with metamorphic fluids, e.g. permeable rocks layers, structural channels (e.g. vein-fractures, shear zones); whereas, preservation of *HP-LT* mineral assemblages occurs in the parts of a rock volume that have been dry (Matthews & Schliestedt, 1984; Parra et al., 2002). Less commonly, metamorphic fluids preserve *HP-LT* mineral assemblages by maintaining a fluid composition which stabilises the *HP-LT* assemblage relative to the replacement assemblage (Kleine et al., 2014). Despite this important kinetic role played by metamorphic fluids, few systematic studies of the interplay between metamorphic fluid flow and other factors (e.g. bulk composition) in controlling replacement and preservation of *HP-LT* mineral assemblages have been undertaken.

Here, we conduct a combined petrological and geochronological study on a spectacular coastal section of the Cyclades Blueschist Unit (CBU) near Fabrika on SE Syros, Greece. At this location, mafic rocks are eclogites, blueschists and greenschists. These rocks alternate with one another on scales of decimetres to 10s of metres. We are able to show that the type of *HP-LT* rock which occurs (eclogite or blueschist) depends on bulk composition. We are also able to show that *HP-LT* rocks were preserved for up to 11–16 million years (probably because metamorphic fluids were absent) before these rocks were locally retrogressed at greenschist facies conditions. These findings raise the question if metamorphic reactions occur to any observable extent in the absence of a fluid.

2 | GEOLOGICAL BACKGROUND

The tectono-metamorphic evolution of Syros and the wider Cyclades is described in several recent reviews (e.g. Jolivet & Brun, 2010; Ring et al., 2010). Syros is located in the back-arc of the presently active Hellenic subduction zone. The rocks on Syros belong to the CBU, a sequence of volcano-sedimentary rocks with preserved evidence of subduction-type *HP-LT* metamorphism. In the Cyclades, the CBU experienced widespread prograde/peak blueschist-eclogite facies metamorphism between 53 and 30 Ma (Ring et al., 2007a, b, 2011; Tomaschek et al., 2003; Wijbrans et al., 1990) and at least two separate localised retrograde greenschist facies metamorphic overprints in the Oligocene (Peillod et al., 2017) and Miocene (Jolivet & Brun, 2010; Ring et al., 2010; Wijbrans & McDougall, 1988).

The CBU on Syros comprises a structurally lower volcano-sedimentary sequence of marbles, metabasalts and other metavolcanics and a structurally higher ophiolitic melange with metabasalts and metamorphosed ultramafic rocks (Keiter et al., 2011). The upper and lower sequences experienced peak *HP-LT* metamorphism at different times: the upper sequence at 53–50 Ma (Tomaschek et al., 2003) and the lower sequence at c. 40 Ma (Cliff et al., 2017). Peak metamorphism produced blueschists and eclogites at estimated *P-T* conditions of 1.5–2.0 GPa and 500–550°C (Trotet et al., 2001; Schumacher et al., 2008; Philippon et al., 2013). The lower sequence is seen on SE Syros below felsic gneiss, chlorite-bearing schists and amphibolite of the Vari unit (Laurent et al., 2016; Ring et al., 2003; Soukis & Stöckli, 2013 did the most detailed study here). Here, blueschists and eclogites alternate with greenschist facies rocks. The timing of greenschist facies metamorphism is not well constrained. However, Maluski et al. (1987) published an Ar-Ar age of c. 30 Ma for greenschist facies mylonitization in the shear zone which borders the Vari unit just E of Fabrika. Also, Bröcker et al. (2013) published a maximum Rb-Sr age for greenschist facies metamorphism in S Syros of c. 21 Ma as well as Ar-Ar and Rb-Sr data which they interpreted as reflecting continuous partial resetting of white micas at greenschist facies conditions.

Previous workers have recognised metamorphic fluid flow events that have affected rocks on Syros and the wider Cyclades which are associated with prograde/peak metamorphism and retrograde metamorphism. These fluids have facilitated metasomatic reactions (e.g. Breeding et al., 2004; Pogge von Strandmann et al., 2015), retrograde metamorphism (e.g. Schliestedt & Matthews, 1987), preservation of *HP-LT* mineral assemblages (Kleine et al., 2014) and multiple stages of veining (Ganor et al., 1994).

3 | METHODS

The coastal section was mapped at a scale of 1:3000 and samples of each of the main rock types were collected for further studies. Transitions between eclogite, blueschist and/or greenschist at scales ranging from decimetres to 10s of metres were described in the field and petrographically.

3.1 | Whole rock chemistry

Whole rock chemistry was determined by inductively coupled plasma mass spectrometry (ICP-MS) at Activation Laboratories in Ontario, Canada. Repeated analysis of standard reference material ensures a accuracy better than 1%. Volatile components are reported as loss on ignition (LOI).

3.2 | Geothermobarometry

Mineral chemistry was determined by electron microprobe (EMP) analysis using a JEOL JXA-8530 field emission electron microprobe at Uppsala University with running conditions of 15 kV and 20 nA and a beam size ranging from 0.5 to 10 μm.

The computer program AX2 (Powell & Holland, 1994) was used to calculate activities of end-member phases from mineral chemistry data. The average PT method of the computer program THERMOCALC (Powell & Holland, 1994) was used to estimate pressure and temperature from activities using dataset 5.5 (Powell et al., 1998). This method returns a *P-T* estimate with uncertainties and diagnostic parameters. The diagnostic parameter σ_{fit} which is a measure of the consistency of the *P-T* estimate with the input data (enthalpies, activities) was used to eliminate unreliable results. Only values for which σ_{fit} is below the threshold value for 95% confidence are reported. We set X_{CO2} = 0.002 based on our pseudosection analysis (see below). This was achieved by setting X_{H2O} = 0.998 for stable assemblages which lacked carbonate minerals. Setting X_{H2O} = 1 for these assemblages had negligible effect on *P-T* estimates.

3.3 | Pseudosections

Pseudosections were constructed using Perple_X 6.8.1 (Connolly, 2005, 2009) with the thermodynamic data set of Holland and Powell (2011; hp11ver.dat) in the system Na_2O–CaO–K_2O–FeO–MgO–Al_2O_3–SiO_2–H_2O–TiO_2–O_2 + CO_2 (NCKFMASHTO+CO_2). Whole rock chemical data were modified to calculate pseudosections at peak metamorphic conditions by extracting the averaged garnet core composition and apatite. We constructed two types of pseudosection: one with H_2O saturated and one with the amount of H_2O defined so that the rock was H_2O saturated at peak metamorphic conditions. In the first type of pseudosection, we set X_{CO2} = 0.002 and O_2 = 1.5 wt.%. because with these values, *P-T*, *P-CO₂* and *T-O₂* pseudosections most closely predicted observed mineral assemblages and proportions. The selected value of X_{CO2} is close to the range 0.005 to 0.03 estimated for glaucophane-bearing marbles from Syros by Schumacher et al. (2008). We used activity–composition models by White et al., (2007) for garnet, White et al., (2010) for ilmenite, White et al., (2014) for white mica, Green et al. (2007) for clinopyroxene, Green et al. (2016) for amphibole, Holland & Powell (1998) for talc, Holland & Powell (2003) for plagioclase and Holland & Powell (2011) for epidote.

3.4 | Geochronology

Mineral separates were prepared for Rb-Sr isotope analysis using small (<100 g) and lithologically homogeneous samples containing white mica as a high Rb/Sr phase. Samples were carefully disintegrated, to retain the original grain size distribution of the mica population. Different minerals and mineral fractions were separated based on density contrasts, distinct magnetic properties, grain shapes and grain size. Mica concentrates were first sieved, to separate different grain size fractions. After that, mica grain size fractions were ground in ethanol in a polished agate mortar and sieved again to obtain inclusion-free separates. All other mineral separates were visually checked and purified by handpicking under a binocular microscope. For analysis, mineral sample weights were typically 5–15 mg for white mica, 20 mg for feldspar, amphibole and omphacite, and between 1 and 10 mg for Sr-rich phases like apatite and epidote-group minerals.

Isotopic data were generated at GFZ Potsdam. Rb and Sr concentrations were determined by isotope dilution using a set of mixed ^{87}Rb-^{84}Sr spikes. After dissolution in a mixture of HF and HNO_3, samples were processed by standard HCl-based cation exchange elution techniques. Isotopic ratios were measured using a Thermo Scientific TRITON thermal ionisation mass spectrometer. Sr isotopic composition was measured in dynamic multicollection mode. Rb isotope dilution analysis was done in static multicollection mode. The value obtained for ^{87}Sr/^{86}Sr in the NIST SRM 987 isotopic standard during the period of analytical work was 0.7102445 ± 0.0000057 (n=10). For age calculation, standard uncertainties, as derived from replicate analyses of spiked white mica samples, of ±0.005% for ^{87}Sr/^{86}Sr and of ±1.5% for ^{87}Rb/^{86}Sr ratios were assigned to the results. Individual analytical uncertainties were consistently smaller than these values. Handling of mineral separates and analytical procedures are described in more detail in Glodny et al. (2008b). Uncertainties of isotope and age data are quoted at 2σ throughout this work. The program ISOPLOT/ EX 3.71 (Ludwig, 2009) was used to calculate regression lines. The ^{87}Rb decay constant is used as recommended by IUPAC-IUGS (Villa et al., 2015).

For Rb-Sr dating we employed the Rb-Sr internal mineral isochron approach using bulk mineral separates from small, visually homogeneous rock samples. Rb–Sr mineral data are well suited to directly date metamorphic processes, like assemblage crystallization, ductile deformation or fluid-induced recrystallisation, in white mica-bearing metamorphic rocks. In the case of high-pressure rocks, texturally complete eclogitization, or conversion of metabasic lithologies to blueschists has been shown to induce Sr-isotopic equilibration, which facilitates Rb-Sr dating of high-pressure metamorphism (Glodny et al., 2002, 2003). Deformation-induced recrystallisation of white mica and associated phases will commonly lead to complete Sr-isotopic re-equilibration and resetting of ages (Inger & Cliff, 1994).

Either partial or complete resetting of ages is also achieved by fluid-induced re-equilibration of formerly metastable assemblages (Glodny et al., 2003). Such reset ages date the last recrystallisation-driving processes, i.e., the waning stages of deformation and fabric formation (Freeman et al., 1998), or completion of reactive assemblage re-equilibration (Glodny et al., 2003), provided that no later thermal-diffusive or retrogressive reactive overprint occurred. Diffusional resetting of the Rb–Sr system in white mica is significant only at very high temperatures of around 600 °C and above (cf. Glodny et al., 2008b). In our study area, peak blueschist- to eclogite facies metamorphic temperatures were generally lower, so that post-crystallisation diffusional resetting of isotopic signatures can largely be ruled out. We analysed white mica in different grain size fractions, to check for the possible presence of mixed mica populations, i.e., of out-of-equilibrium, detrital, pre- or early-deformational white mica relicts (cf. Müller et al., 1999).

In samples showing incomplete Sr-isotopic re-equilibration, Sr isotopic inhomogeneities are the reflection of incomplete recrystallization or presence of relict grains (e.g. Cliff et al., 2017). A common pattern here is a positive correlation between white mica grain size and apparent ages, with higher apparent ages for larger grain size fractions. This observation is consistent with grain size sensitivity of several ductile deformation mechanisms (Platt & Behr, 2011) and the observation that fluid induced re-equilibration tends to start from cracks and grain boundaries (Straume & Austrheim, 1999), affecting predominantly small grains and grain rims while leaving the interior of big grains as relicts of the early stages of transformation. Therefore, this type of correlation suggests either a prolonged deformation- or fluid-related recrystallization process (i.e., apparently older white mica grains crystallized during the early metamorphic stages) or partial isotopic inheritance from the precursor rock (Angiboust et al., 2014, 2016). In consequence, the smallest mica crystals in a given rock will commonly be most readily affected by dynamic recrystallisation processes or late, fluid-limited recrystallisation, and show isotopic signatures most closely associated to the last event of ductile deformation or fluid activity. Apparent ages for small grain size mica fractions can thus be considered as the maximum age of the last deformation or reactive overprint in a given sample.

4 | FIELD RELATIONS

The coastal section is shown in figure 1. Mafic layers alternate with massive pale-coloured quartz-carbonate units along the entire section. The section is divided by a 50-m-wide zone bearing 1-2-m-diameter eclogite facies ultramafic knockers with 10-cm greenschist/blueschist facies rinds (Figures 2a–c), which we interpret to represent a shear zone.

Two types of quartz-carbonate units were observed, one of which contained abundant white mica and 5–20 mm garnet porphyroblasts with retrograde chlorite rims. The other lacked garnet porphyroblasts and contained only small amounts of white mica.

We classified the mafic rocks as eclogite, blueschist or greenschist based on their appearance in the field. The eclogites are fine-grained and vivid green in colour with garnet porphyroblasts ranging in size from 1 to 10 mm (Figure 3a). Some eclogites also contain up to 10-mm-long prisms of glaucophane (Figure 3b). The blueschists are fine-grained and blue in colour with garnet porphyroblasts ranging in size from 1 to 10 mm and up to 10-mm-long prisms of epidote in a fine-grained vivid or dark blue matrix (Figure 3c). The greenschist is greyish green in colour with albite porphyroblasts, ranging in size from 2 to 5 mm (Figure 3d).

The best preserved eclogites are found at either end of the studied coastal section. At the SW end of the section, compositional layering with alternating 5-10-cm thick mafic and carbonate-quartz layers can be seen (Figure 4a). At the NE end of the section, eclogites are cross-cut by numerous cm-m-wide dolomite veins. At the SW end of the section, veining is much less extensive. Partial replacement of eclogite by blueschist or greenschist occurs alongside quartz-carbonate veins producing 1–2 cm wide halos (Figures 4b–c).

The eclogites at the SW end of the section are structurally overlain by a section which is dominated by layered blueschists (Figure 1). Blueschist layers alternate with layers of eclogite and quartz-carbonate rocks (Figure 5a). Replacement by greenschist alongside quartz-carbonate veins is also seen in these rocks (Figures 5b–c).

The blueschists are structurally overlain by a section which is dominated by greenschist (Figure 1). This section, which extends as far as the zone of eclogite knockers, consists mainly of massive greenschist that lack discernible layering (Figure 6a) but contains 30–50 cm pods of monomineralic epidote. In some parts of this section, remnants of a former eclogite assemblage are seen, e.g. by garnet at the cores of albite porphyroblasts (Figure 6b). Elsewhere eclogite and blueschist are preserved alongside quartz-carbonate layers (Figure 7a) and blueschist is preserved alongside a quartz-carbonate vein (Figure 7b), an association which was first described by Kleine et al. (2014).

5 | SAMPLE DESCRIPTIONS

5.1 | Eclogites

Samples 17FB06, 15SY03 and 15SY05 (located on figure 1) are, based on their appearance in the field, eclogites. All samples were examined petrographically and EMP analysis was performed on sample 15SY03. Representative mineral analyses are listed in table 1 and mineral modes are listed in table 2. This sample contains garnet, clinopyroxene (omphacite), amphibole (glaucophane), white mica (phengite: Si ~3.4 a.p.f.u.), epidote (X_{cz} ~0.8), rutile, apatite, quartz and calcite (Figures 8a,b). Garnet cores show decreasing spessartine and increasing pyrope contents (Figure 9a) which we infer indicates prograde growth. They contain abundant inclusions of glaucophane, jadeite, paragonite, epidote and albite. Garnet rims show increasing spessartine and decreasing pyrope contents (Figure 9a) from which we infer retrogression. The rim contains inclusions of glaucophane, omphacite, paragonite and epidote. The outer part contains few inclusions. Some garnets have an outer rim with decreasing spessartine and increasing pyrope contents (Figure 9a), which is largely free from inclusions. Some garnets contain inclusions, which based partly on their diamond shape, we infer to be former lawsonite, now entirely pseudomorphed by epidote (X_{cz} ~0.8), paragonite and albite (Figure 8g). Calcite replaces omphacite, glaucophane and epidote (Figure 8h) and forms grain boundary films around other mineral grains implying that calcite formed later than the other minerals, probably in response to fluid-driven carbonation. This was also suggested by Kleine et al. (2014).

5.2 | Blueschists

Samples 15SY01 and 15SY02 (located on Figure 1) are, based on their appearance in the field, blueschists. Petrographic and EMP analysis (Table 1) of sample 15SY01 show that it contains garnet, clinopyroxene (omphacite), amphibole (glaucophane), epidote, white mica (paragonite and phengite: Si ~3.4 a.p.f.u.), calcite, rutile and quartz (Figures 8c,d). Garnet cores show decreasing spessartine and increasing pyrope contents (Figure 9b). They contain abundant inclusions of glaucophane, aegirine augite, paragonite, phengite and epidote. Some garnet rims show increasing spessartine and decreasing pyrope contents (Figure 9b) which we infer indicates retrogression. The rim contains inclusions of glaucophane, omphacite, paragonite and epidote. The outer part contains inclusions of glaucophane, omphacite, paragonite and epidote. Some garnets have an outer rim which is largely free from inclusions. The garnets contain former lawsonite, now entirely pseudomorphed by epidote (X_{Cz} ~0.8) and white mica (paragonite and phengite: Si ~3.4 a.p.f.u.). We note that the blueschist contains the same minerals as the eclogite samples, but in different proportions (Table 2). Also, based on similar textures to those observed in the eclogite samples, calcite formed later, probably in response to fluid-driven carbonation.

5.3 | Greenschists

Samples 17FB03 and 17FB05 (located on figure 1) are, based on their appearance in the field, greenschists. Petrographic and EMP analysis of sample 17FB03 show that it contains amphibole (actinolite), chlorite, epidote, albite titanite, apatite and quartz (Figures 8e,f). The sample also contains garnets which are partly replaced by chlorite or rimmed by albite (Figures 8e,f), white mica (phengite) which is partly replaced by chlorite, and rutile which is rimmed by titanite. Also, cores of some actinolite grains are composed of winchite. The garnets occur in fragments but some of these show decreasing spessartine and increasing pyrope contents (Figure 9c), similar to the blueschist and eclogite samples, from which infer prograde growth.

6 | *P-T*-t ESTIMATES

P-T estimates obtained from samples 15SY03 (eclogite), 15SY01 (blueschist) and 17FB03 (greenschist) are listed in table 3 and shown in figure 10. For the eclogite and blueschist samples, separate *P-T* estimates were obtained from 1) garnet cores and mineral inclusions, 2) garnet inner rims and mineral inclusions, and 3) garnet outer rims and matrix minerals. Equilibrium was supported by multiphase inclusions. Metamorphic ages (t) are shown in figure 11 with supporting data in table 4. These were determined for samples 15SY03 (eclogite), 15SY05 (eclogite), 15SY01 (blueschist) and 17FB05 (greenschist), which was collected from the same outcrop as sample 17FB03.

6.1 | Eclogites

From sample 15SY03, we obtained *P-T* estimates of 1.14 ± 0.07 GPa and 398 ± 15 °C for the garnet core, co-existing inclusions (amphibole, clinopyroxene, white mica, plagioclase, epidote, rutile and quartz) and lawsonite; 1.97 ± 0.10 GPa and 536 ± 17 °C for the garnet inner rim, co-existing inclusions (amphibole, clinopyroxene, white mica, plagioclase, epidote, rutile and quartz) and lawsonite; and 1.59 ± 0.19 GPa and 513 ± 39°C for the garnet outer rim and matrix minerals (Figure 10).

From sample 15SY03, we obtained a Rb-Sr age of 39.6 ± 1.2 Ma using epidote, amphibole (glaucophane), clinopyroxene (omphacite) and white mica grain size fractions (Figure 11a). There is a correlation between white mica grain sizes and Rb/Sr ratios, possibly related to the metamorphic reaction history, but no correlation between grain sizes and apparent ages is observed. We infer that the Rb-Sr age we obtained from this sample dates eclogite formation at that time. From sample 15SY05, we obtained a Rb-Sr age of 41.6 ± 1.5 Ma using epidote, amphibole (glaucophane), clinopyroxene (omphacite), apatite and white mica grain size fractions (Figure 11b). This age is, within limits of 2σ uncertainty, identical to that of sample 15SY03. In both samples there are slight Sr-isotopic disequilibria between the low-Rb/Sr phases. It remains unclear whether these disequilibria were inherited from pre-eclogite facies precursor phases or whether they represent incipient post-eclogite facies retrogression. In any case, the age information is robust within limits of stated uncertainties. We also note that initial Sr isotopic composition of the two eclogite samples are, within limits of uncertainty also the same ($^{87}Sr/^{86}Sr$ = 0.7057), indicating that these two samples can have had similar protolith sources.

6.2 | Blueschists

From sample 15SY01, we obtained *P-T* estimates of 1.28 ± 0.15 GPa and 436 ± 24 °C for the garnet core, co-existing inclusions (amphibole, clinopyroxene, white mica, plagioclase, epidote, rutile and quartz) and lawsonite; 1.88 ± 0.11 GPa and 540 ± 19 °C for the garnet inner rim, co-existing inclusions (amphibole, clinopyroxene, white mica, plagioclase, epidote, rutile and quartz) and lawsonite; and 1.36 ± 0.25 GPa and 519 ± 46 °C for the garnet outer rim and matrix minerals (Figure 10).

The same sample gave a well-constrained Rb-Sr age of 41.36 ± 0.45 Ma from epidote, amphibole (glaucophane), clinopyroxene (omphacite), apatite and white mica grain size fractions (Figure 11). The initial Sr isotopic composition is very similar to that of the two eclogite samples (15SY03 and 15SY05), which again implies similar protolith sources. The age of 41.36 ± 0.45 Ma is within limits of uncertainty, identical to the eclogite samples. We infer that the same metamorphic event at 38–43 Ma (41.2 ± 1.7 Ma (weighted mean, 2σ)) is dated by blueschist and eclogite mineral assemblages.

6.3 | Greenschists

From sample 17FB03, we obtained a *P-T* estimate of 0.34 ± 0.21 GPa and 456 ± 68 °C for the greenschist facies assemblage (Figure 10).

Rb-Sr data for the greenschist sample 17FB05 show marked Sr isotopic disequilibria among different minerals and mica grain size fractions. Formally, the age obtained from the mineral data is 30.8 ± 2.1 Ma (Figure 11d). There is a correlation between white mica grain size and apparent age. Larger grains of white mica plot above the regression line, implying that large-size white mica may contain inherited domains or incompletely re-equilibrated Sr, whereas more fine grained white mica plots below the regression line, indicating late recrystallization. This disequilibrium in the white mica population is paralleled by disequilibria between the low-Rb/Sr phases. Apatite and epidote have low $^{87}Sr/^{86}Sr$ ratios, indicating that these phases may be at least partly inherited from the *HP-LT* eclogite/blueschist precursor rock. In contrast, actinolite and albite have higher $^{87}Sr/^{86}Sr$, suggesting that these phases grew late in the reaction history of the rock. From these phases and the more fine-grained white mica fraction we can estimate that greenschist facies reworking ended at (or shortly after) 26.9 ± 0.4 Ma (Figure 11d).

7 | BULK COMPOSITIONS AND PSEUDOSECTIONS

Similar *P-T* conditions were calculated from eclogite and blueschist samples (Figure 10). Also, age determinations indicate that eclogite and blueschist formed at the same time at similar *P-T* conditions (Figure 11). This suggests that the occurrence of eclogite and blueschist reflects different bulk compositions. Whole rock chemical analyses of mafic rocks (eclogite, blueschist and greenschist) and a carbonate layer between eclogite layers are shown in Table 5. These data confirm that while bulk compositions of eclogite, blueschist and greenschist are similar with respect to some major element oxides, the eclogite sample (15SY03) contains more K_2O, Al_2O_3 and Fe_2O_3(T) and less MgO than the blueschist and greenschist samples (15SY01 and 17FB03, respectively). The effect of this difference in bulk composition on modal mineralogy was tested by constructing *P-T* pseudosections for the eclogite (15SY03) and blueschist (15SY01) samples firstly at H_2O saturation (Figures 12a,b). Stability fields for amphibole + clinopyroxene + white mica + garnet + epidote + rutile + quartz, i.e. the observed mineral assemblages of the eclogite and blueschist samples, are observed on both *P-T* pseudosections. These overlap at *P* = 1.5–2.1 GPa and *T* = 510–580 ºC. Mineral modes estimated from isopleths are similar to estimates made by point counting (Table 2). The observed modal differences between the eclogite (contains 9-11 vol. % more omphacite and 21-25 vol. % more mica) and blueschist (contains 27-30 vol. % more amphibole and 9-12 vol. % more epidote) are closely replicated by the *P-T* pseudosections. There is some overlap between peak metamorphic *P-T* conditions estimated from the *P-T* pseudosections and *P-T* estimates for prograde and peak metamorphic stages made using the average *PT* method of THERMOCALC (Figure 10). Differences probably reflect shortfalls of the underlying assumptions of both approaches, i.e. that equilibrium between phases used to estimate *P* and *T* using THERMOCALC was attained and/or that the bulk composition used to construct the *P-T* pseudosections was representative of the volume of rock within which equilibrium was attained. However, some overlap between *P-T* estimates made using different approaches, as well as similarity between our findings and previous work (Schumacher et al., 2008; Philippon et al., 2013) are encouraging.

8 | DISCUSSION

Rocks from our study area on Syros preserve evidence of three metamorphic stages. Similar prograde (lawsonite blueschist) and peak (blueschist/eclogite facies) metamorphic stages are recorded by both eclogites and blueschists. There is also evidence of a retrograde (greenschist facies) stage which is recorded locally.

8.1 | Eclogites and blueschists

Based on field observations of mafic/carbonate/clastic compositional layering (Figures 4a,5a), we interpret that the main protolith of the metamorphic sequence which was studied on SE Syros was a layered sequence of mafic volcanic and carbonate/clastic sediments. Mafic rocks are now eclogites, blueschists and greenschists. Eclogites and blueschists record similar *P-T* histories (Figures 10,12) with 1) prograde metamorphism at lawsonite blueschist facies conditions (*P* = 1.2–1.9 GPa and *T* = 410–530°C: based on estimates made using the average PT method of THERMOCALC) and 2) peak metamorphism at blueschist/eclogite facies conditions (*P* = 1.5–2.1 GPa, *T* = 520–580°C: based on the *P-T* pseudosections). Peak metamorphism of eclogite and blueschist was synchronous, occurring at 41.2 ± 1.7 Ma (Figures 11a–c).

The similar *P-T*-t histories of eclogite and blueschist in our study area on Syros point to bulk composition (rather than *P-T*) variation as the reason for co-existence of eclogite and blueschist. This is supported by the observation of alternating eclogite and blueschist layers (Figure 5a) which suggests that their co-existence reflects an original compositional layering. In our study, eclogite contains higher proportions of Fe_2O_3(T), Al_2O_3, and K_2O whereas the blueschist contains a higher proportion of MgO and Na_2O. Also, eclogites and blueschists contain the same minerals but in different proportions (Table 2). Pseudosections constructed for eclogite and blueschist samples (Figure 12) confirm that observed differences in modal mineralogy can be explained by measured differences in bulk composition. Compositional variation has been put forward as an explanation for co-existence of eclogite and blueschist in several previous studies. Gomez-Pugnaire et al. (1997) argued that higher $Na_2O/(Na_2O$ + CaO) favours blueschist rather than eclogite in the Nerkan Complex (Urals). Brovarone et al. (2011) put forward a similar argument for co-existence of lawsonite-bearing eclogites and blueschists in Alpine Corsica (France) but they imply that higher CaO proportions in general favour eclogites. Likewise, Wei & Clarke (2011) argued that co-occurrence of low-T eclogite and blueschist may result from compositional differences with higher CaO proportions favouring eclogite. As supporting evidence, they cited co-occurrence of eclogite (with a higher CaO proportion) and blueschist (with a lower CaO proportion) in the Sivrihisar Massif, Turkey, reported by Davis & Whitney (2006). The importance of CaO for stabilising eclogite is also inferred by Tian and Wei (2014) for co-existing eclogite and garnet blueschist in Tianshan (China). Our findings differ in that eclogites and blueschists from our study area contain similar proportions of CaO and variations of other major element oxide concentrations are of seemingly greater importance. Specifically, higher proportions of FeO and Al_2O_3, and a 5 times higher proportion of K_2O favour eclogite; whereas, a higher proportion of Na_2O and a 2 times higher proportion of MgO favour blueschist.

8.2 | Greenschists

Greenschists from our study area record retrograde metamorphism at *P* = 0.34 ± 0.21 GPa and *T* = 456 ± 68 °C (Figure 10) which ended at (or slightly after) 27 Ma (Figure 11d). This was spatially restricted. The mapped outcrop pattern (Figure 1) suggests that on a scale of 10-100-m retrograde metamorphism was obliquely centred on a poorly exposed section with eclogite facies ultramafic knockers which we infer to be a gently dipping shear zone. This is consistent with retrogression having been caused by fluid flow channelled along the shear zone. This interpretation is also supported by retrograde blueschist/greenschist facies rinds enveloping the knockers (Figure 2). Spatial coupling of retrogression and fluid flow is also seen on a scale of 1-10-cm. For example, fluids have exploited structural pathways (Figures 4b,5b) causing local replacement of eclogite and blueschist by greenschist facies minerals alongside veins (Figures 4c,5c). Interestingly, not only replacement but also preservation of specifically blueschist is associated with proximity to fluid pathways (Figure 7b). This was shown to be related to fast flowing high X_{CO2} fluids (Kleine et al., 2014), implying that both fluid flux and fluid composition has controlled the spatial extent of retrograde metamorphism.

Greenschist facies metamorphism occurred up to 11–16 million years after peak metamorphism This implies a period of metamorphic quiescence after blueschist/eclogite facies metamorphism that may have lasted for up to 11–16 million years, before greenschist facies reworking. The association of greenschist facies retrogression with a shear zone on a scale of 10-100-m and veins on a scale of 1-10-cm implies that retrogression only occurred when and where metamorphic fluids were present. This requirement is further emphasised by *P-T* pseudosections calculated with a given amount of H_2O, chosen so that the rock was H_2O saturated at peak metamorphic conditions (Figures 12c,d). These pseudosections show that H_2O becomes undersaturated during decompression and cooling underpinning the need for an external metamorphic fluid to facilitate retrogression (cf. Pitra et al., 2010).

8.3 | Tectonic implications

The age of *HP-LT* metamorphism in SE Syros of 38–43 Ma obtained in this study is similar to a previous estimate (c. 40 Ma) from the same tectonic unit on Syros (Cliff et al., 2017; Uunk et al., 2018), but differs from age estimates (c. 50 Ma) from the a structurally higher ophiolitic melange also on Syros (Tomaschek et al., 2003) and age estimates (c. 30 Ma) from a structurally lower unit on Evia (Ring et al., 2007a) and Sifnos (Ring et al., 2011; Wijbrans et al., 1990). These results imply that the Cyclades Blueschist Unit comprises at least three distinct *HP-LT* metamorphic belts of different ages. This indicates that the Cyclades Blueschist Unit is a subduction-related nappe stack.

The approximate age of 27 Ma obtained in this study for the end of greenschist facies reworking corroborates a similar age determination obtained from rocks on Naxos (Peillod, 2018). This Oligocene greenschist-facies event is a new finding in the Cyclades area. It precedes widespread Miocene metamorphism associated with Aegean-wide extensional deformation. Maluski et al. (1987) suggested that their Ar/Ar age of 30 Ma is related to the emplacement of the greenschist-facies Vari Unit above the CBU. If so, this tectonic event could have triggered fluid flow leading to the greenschist facies overprint of the CBU at Fabrika.

Our new age data also show that while the lowermost nappes of the Cyclades Blueschist Unit were undergoing *HP-LT* metamorphism at c. 30 Ma e.g. on Sifnos (Ring et al., 2011), rocks on SE Syros were already at greenschist facies conditions. This close association of *HP-LT* metamorphism at lower structural levels and greenschist facies conditions at higher structural levels implies that exhumation was not due to extensive lithospheric back-arc extension but occurred within the subduction zone itself. This supports the hypothesis that the Cyclades Blueschist Unit was initially exhumed in extrusion wedges as demonstrated by Ring et al. (2007a, 2007b) and inferred by Huet et al. (2009); Ring et al. (2011) and Peillod (2018).

Finally, the age difference between *HP-LT* and greenschist facies metamorphism recorded by rocks from SE Syros is probably 11–16 Ma and the difference in metamorphic pressure demands exhumation of ~50 km (assuming an average rock density of 2700–3000 kg m^{-3}), resulting in time-averaged exhumation rates of 3–4 km/million years. More importantly in a tectonometamorphic context is that we provided evidence that the eclogite/blueschist sequence was largely unaffected by metamorphic reactions during exhumation. The rocks were only affected by greenschist facies metamorphism alongside a shear zone which likely provided a pathway for metamorphic fluid flow at that time. This raises a fundamental question: Do metamorphic reactions occur to any observable extent in the absence of a fluid?

9 | CONCLUSIONS

We conclude that eclogites and blueschists near Fabrika on SE Syros experienced similar metamorphic histories. Both rock types record a prograde lawsonite blueschist facies stage at 1.2–1.9 GPa and 410–530 °C, and a peak blueschist/eclogite facies stage at 1.5–2.1 GPa and 520–580 °C. The latter stage occurred at 43–38 Ma. The co-existence of eclogites and blueschists is explained by compositional variation probably reflecting original layering. Greenschist facies retrogression at 0.34 ± 0.21 GPa and T = 456 ± 68 °C was spatially associated with fluid channels: a shear zone (on a 10-100-m scale), and veins (on a 1-10-cm scale). We infer that greenschist facies retrogression was fluid-induced. Also, greenschist facies retrogression occurred up to 11–16 million years after eclogite/blueschist facies metamorphism and may have been associated with fluid flow related to emplacement of the Vari Unit above the CBU. The inferred period of metamorphic quiescence implies that in the case of retrograde metamorphism, reactions are extremely sluggish or simply do not occur in the absence of a fluid.

ACKNOWLEDGEMENTS

Pavel Pitra, John Schumacher and Donna Whitney are thanked for constructive and thoughtful reviews and editorial handling. The late Dan Zetterberg is acknowledged for sample preparation. The authors have no conflicts of interest.

REFERENCES

Angiboust, S., Agard, P., Glodny, J., Omrani, J., & Oncken, O. (2016). Zagros blueschists: Episodic underplating and long-lived cooling of a subduction zone. *Earth and Planetary Science Letters*, *443*, 48–58.

Angiboust, S., Glodny, J., Oncken, O., & Chopen, C. (2014). In search of transient subduction interfaces in the dent blanche-sesia tectonic system (W. Alps). *Lithos*, *205*, 298–321.

Austrheim, H. (1987). Eclogitization of lower crustal granulites by fluid migration through shear zones. *Earth and Planetary Science Letters*, *81*, 221–232.

Baldwin, J. A., Bowring, S. A., Williams, M. L., & Williams, I. S. (2004). Eclogites of the Snowbird tectonic zone: Petrological and U-Pb geochronological evidence for Paleoproterozoic high-pressure metamorphism in the western Canadian Shield. *Contributions to Mineralogy and Petrology*, *147*, 528–548.

Breeding, C. M., Ague, J. J., Bröcker, M., & Bolton, E. W. (2003). Blueschist preservation in a retrograded, high-pressure, low-temperature metamorphic terrane, Tinos, Greece: Implications for fluid flow paths in subduction zones. *Geochemistry, Geophysics, Geosystems*, *4*, 9002.

Breeding, C. M., Ague, J. J., & Bröcker, M. (2004). Fluid-metasedimentary rock interactions in subduction-zone mé lange: Implications for the chemical composition of arc magmas. *Geology*, *32*, 1041–1044.

Brovarone, A. V., Groppo, C., Hetényi, G., Compagnoni, R., & Malavieille, J. (2011). Coexistence of lawsonite-bearing eclogite and blueschist - phase equilibria modelling of Alpine Corsica metabasalts and petrological evolution of subducting slabs.pdf. *Journal of Metamorphic Geology*, *29*, 583–600.

Bröcker, M, Baldwin, S., & Arkudas, R. (2013). The geological significance of $^{40}Ar/^{39}Ar$ and Rb–Sr white mica ages from Syros and Sifnos, Greece: a record of continuous (re)crystallization during exhumation? *Journal of Metamorphic Geology*, *31*, 629–546.

Cliff, R. A., Bond, C. E., Butler, R. W. H., Dixon, J. E. (2017). Geochronological challenges posed by continuously developing tectonometamorphic systems: insights from Rb–Sr mica ages from the Cycladic Blueschist Belt, Syros (Greece). *Journal of Metamorphic Geology*, *35*, 197–211.

Connolly, J. A. D. (2005). Computation of phase equilibria by linear programming: a tool for geodynamic modeling and its application to subduction zone decarbonation. *Earth and Planetary Science Letters*, *236*, 524–541.

Connolly, J. A. D. (2009). The geodynamic equation of state: what and how. *Geochemistry, Geophysics, Geosystems*, *10*, Q10014.

Davis, P. B., & Whitney, D. L. (2006). Petrogenesis of lawsonite and epidote eclogite and blueschist, Sivrihisar, Turkey. *Journal of Metamorphic Geology*, *24*, 823–849.

Ernst, W. G. (1988). Tectonic history of subduction zones inferred from retrograde blueschist

PT paths. *Geology*, *16*, 1081–1084.

Freeman, S. R., Butler, R. W. H., Cliff, R. A., & Rex, D. C. (1998). Direct dating of mylonite evolution: a multi-disciplinary geochronological study from the Moine Thrust Zone, NW Scotland. *Journal of the Geological Society*, *155*, 745–758.

Ganor, J., Matthews, A., & Schliestedt, M. (1994). Post-metamorphic low δ13 C calcite in the Cycladic complex (Greece) and their implications for modeling fluid infiltration processes using carbon isotope compositions. *European Journal of Mineralogy*, *6*, 365–380.

Glodny, J., Austrheim, H., Molina, J. F., Rusin, A. I., & Seward, D. (2003). Rb/Sr record of fluid-rock interaction in eclogites: The Marun-Keu complex, Polar Urals, Russia. *Geochimica et Cosmochimica Acta*, *67*, 4353–4371.

Glodny, J., Bingen, B., Austrheim, H., Molina, J. F., & Rusin, A. (2002). Precise eclogitization ages deduced from Rb/Sr mineral systematics: the Maksyutov complex, Southern Urals, Russia. *Geochimica et Cosmochimica Acta*, *66*, 1221–1235.

Glodny, J., Kühn, A., & Austrheim, H. (2008a). Geochronology of fluid-induced eclogite and amphibolite facies metamorphic reactions in a subduction-collision system, Bergen Arcs, Norway. *Contributions to Mineralogy and Petrology*, *156*, 27–48.

Glodny, J., Ring, U., & Kühn, A. (2008b). Coeval high-pressure metamorphism, thrusting, strike-slip, and extensional shearing in the Tauern Window, Eastern Alps. *Tectonics*, *27*, TC4004.

Gómez-Pugnaire, M. T., Karsten, L., & Sánchez-Vizcaíno, V. L. (1997). Phase relationships and *P-T* conditions of coexisting eclogite- blueschists and their transformation to greenschist-facies rocks in the Nerkau Complex (Northern Urals). *Tectonophysics*, *276*, 195–216.

Green, E. C. R., Holland, T., & Powell, R. (2007). An order-disorder model for omphacitic pyroxenes in the system jadeite-diopside-hedenbergite-acmite, with applications to eclogitic rocks. *American Mineralogist*, *92*, 1181–1189.

Green, E. C. R., White, R. W., Diener, J. F. A., Powell, R., Holland, T. J. B., & Palin, R. M. (2016). Activity–composition relations for the calculation of partial melting equilibria in metabasic rocks. *Journal of Metamorphic Geology*, *34*, 845–869.

Holland, T. J. B., & Powell, R. (1998). An internally consistent thermodynamic data set for phases of petrological interest. *Journal of Metamorphic Geology, 16,* 309–343.

Holland, T. J. B., & Powell, R. (2003). Activity-composition relations for phases in petrological calculations: an asymmetric multicomponent formulation. *Contributions to Mineralogy and Petrology, 145*, 492–501.

Holland, T. J. B., & Powell, R. (2011). An improved and extended internally consistent thermodynamic dataset for phases of petrological interest, involving a new equation of state for solids. *Journal of Metamorphic Geology, 29*, 333-383.

Huet, B., Labrousse, L., & Jolivet, L. (2009). Thrust or detachment? exhumation processes in the aegean: Insight from a field study on Ios (Cyclades, Greece). *Tectonics*, *28*, TC3007.

Inger, S., & Cliff, R. A. (1994). Timing of metamorphism in the Tauern Window, Eastern Alps: Rb-Sr ages and fabric formation. *Journal of Metamorphic Geology*, *12*, 695–707.

Jolivet, L., & Brun, J. P. (2010). Cenozoic geodynamic evolution of the Aegean. *International Journal of Earth Sciences, 99,* 109–138.

Jun, G., & Klemd, R. (2000). Eclogite Occurrences in the Southern Tianshan High-Pressure Belt, Xinjiang, Western China. *Gondwana Research*, *3*, 33–38.

Keiter, M., Ballhaus, C., & Tomaschek, F. (2011). A new geological map of the island of Syros (Aegean Sea, Greece) - implications for lithostratigraphy and structural history of the Cycladic Blueschist Unit. *Geological Society of America Special Papers*, *481*, 43 pp.

Kleine, B. I., Skelton, A. D. L., Huet, B., & Pitcairn, I. K. (2014). Preservation of Blueschist-facies Minerals along a Shear Zone by Coupled Metasomatism and Fast-flowing CO2-bearing Fluids. *Journal of Petrology, 55*, 1905–1939.

Laurent, V., Jolivet, L., Roche, V., Augier, R., Scaillet, S., & Cardello, G. L. (2016). Strain localization in a fossilized subduction channel: Insights from the Cycladic Blueschist Unit (Syros, Greece). *Tectonophysics*, *672–673*, 150–169.

Ludwig, K. R. (2009). *Isoplot/Ex Ver 3.71: A Geochronological Toolkit For Microsoft Excel*. Berkeley Geochronology Center Special Publication, Berkeley.

Maluski, H., Bonneau, M., & Kienast, J. R. (1987). Dating the metamorphic events in the

Cycladic area; 39Ar/40 Ar data from metamorphic rocks of the Island of Syros (Greece). *Bull. Société Géologique France*, *3*, 833–842.

Matthews, A., & Schliestedt, M. (1984). Evolution of the blueschist and greenschist facies rocks of Sifnos, Cyclades, Greece - A stable isotope study of subduction-related metamorphism. *Contributions to Mineralogy and Petrology*, *88*, 150–163.

Müller, W., Dallmeyer, R.D., Neubauer, F, & Thöni, M. (1999). Deformation-induced resetting of Rb/Sr and 40Ar/39Ar mineral systems in a low-grade, polymetamorphic terrane (Eastern Alps, Austria). *Journal of the Geological Society*, *156*, 261–278.

Parra, T., Vidal, O., & Jolivet, L. (2002). Relation between the intensity of deformation and retrogression in blueschist metapelites of Tinos Island (Greece) evidenced by chlorite-mica local equilibria. *Lithos*, *63*, 41–66.

Peillod, A., Ring, U., Glodny, J., & Skelton, A. (2017). An Eocene/Oligocene blueschist-/greenschist facies P–T loop from the Cycladic Blueschist Unit on Naxos Island, Greece: Deformation-related re-equilibration vs. thermal relaxation. *Journal of Metamorphic Geology*, *35*, 805–830.

Peillod, A. (2018). *The metamorphic history of Naxos (central Cyclades, Greece): Deciphering the Oligocene and Miocene exhumation events*. Unpublished PhD thesis. Department of Geological Sciences, Stockholm University.

Philippon, M. Gueydan, F., Pitra P., & Brun J. P. (2013). Preservation of subduction-related prograde deformation in lawsonite pseudomorph-bearing rocks, *Journal of Metamorphic Geology, 31*, 571–583.

Pitra, P., Kouamelan, A. N., Ballèvre, M., & Peucat, J. J. (2010). Palaeoproterozoic high-pressure granulite overprint of the Archean continental crust: evidence for homogeneous crustal thickening (Man Rise, Ivory Coast). *Journal of Metamorphic Geology*, *28***,** 41–58.

Platt, J. P., & Behr, W. M. (2011). Grainsize evolution in ductile shear zones: Implications for strain localization and the strength of the lithosphere. *Journal of Structural Geology*, *33*, 537–550.

Pogge von Strandmann, P. A. E., Dohmen, R., Marschall, H. R., Schumacher, J. C., & Elliott, T. (2015). Extreme magnesium isotope fractionation at outcrop scale records the mechanism and rate at which reaction fronts advance. *Journal of Petrology*, *56*, 33–

58.

Powell, R., & Holland, T. (1994). Optimal geothermometry and geobarometry. *American Mineralogist*, *79*, 120–133.

Powell, R., Holland, T., & Worley, B. (1998). Calculating phase diagrams involving solid solutions via non-linear equations, with examples using THERMOCALC. *Journal of Metamorphic Geology*, *16*, 577–588.

Proyer, A. (2003). The preservation of high-pressure rocks during exhumation: metagranites and metapelites. *Lithos*, *70*, 183–194.

Ring, U., Glodny, J., Will, T., & Thomson, S. (2007a). An Oligocene extrusion wedge of blueschist-facies nappes on Evia, Aegean Sea, Greece: implications for the early exhumation of high-pressure rocks. *Journal of the Geological Society*, *164*, 637–652.

Ring, U., Glodny, J., Will, T., & Thomson, S. (2010). The Hellenic Subduction System: High-Pressure Metamorphism, Exhumation, Normal Faulting, and Large-Scale Extension. *Annual Review of Earth and Planetary Sciences*, *38*, 45–76.

Ring, U., Glodny, J., Will, T. M., & Thomson, S. (2011). Normal faulting on Sifnos and the South Cycladic Detachment System, Aegean Sea, Greece. *Journal of the Geological Society*, *168*, 751–768.

Ring, U., Thomson, S. N., & Brocker, M. (2003). Fast extension but little exhumation: the Vari detachment in the Cyclades, Greece. *Geological Magazine*, *140*, 245–252.

Ring, U., Will, T., Glodny, J., Kumerics, C., Gessner, K., Thomson, S., Güngör, T., Monié, P., Okrusch, M., & Drüppel, K. (2007b). Early exhumation of high-pressure rocks in extrusion wedges: Cycladic blueschist unit in the eastern Aegean, Greece, and Turkey. *Tectonics*, *26*, 1–23.

Rubatto, D., & Hermann, J. (2001). Exhumation as fast as subduction? *Geology*, *29*, 3–6.

Schliestedt, M., & Matthews, A. (1987). Transformation of blueschist to greenschist facies rocks as a consequence of fluid infiltration, Sifnos (Cyclades), Greece. *Contributions to Mineralogy and Petrology*, *97*, 237–250.

Schorn, S. (2018). Dehydration of metapelites during high-*P* metamorphism: The coupling between fluid sources and fluid sinks. *Journal of Metamorphic Geology*, *36*, 369–391.

Schumacher, J. C., Brady, J. B., Cheney, J. T., & Tonnsen, R. R. (2008). Glaucophane-bearing marbles on Syros, Greece. *Journal of Petrology*, *49*, 1667–1686.

Soukis, K., & Stöckli, D .F. (2013). Structural and thermochronometric evidence for multi-stage exhumation of Southern Syros, Cycladic islands, Greece. *Tectonophysics*, *595*, 148–164.

Straume, Å. K., & Austrheim, H. (1999). Importance of fracturing during retro-metamorphism of eclogites. *Journal of Metamorphic Geology*, *17*, 637–652.

Tian, Z. L., & Wei, C. J. (2014). Coexistence of garnet blueschist and eclogite in South Tianshan, NW China: dependence of *P-T* evolution and bulk-rock composition. *Journal of Metamorphic Geology*, **32**, 743–764.

Tomaschek, F., Kennedy, A. K., Villa, I. M., Lagos, M., & Ballhaus, C. (2003). Zircons from Syros, Cyclades, Greece--Recrystallization and Mobilization of Zircon During High-Pressure Metamorphism. *Journal of Petrology*, *44*, 1977–2002.

Trotet, F., Vidal, O., & Jolivet, L. (2001). Exhumation of Syros and Sifnos metamorphic rocks (Cyclades, Greece). New constraints on the *P-T* paths. *European Journal of Mineralogy*, *13*, 901–920.

Uunk, B., Brouwer, F., Voorde, M., & Wijbrans, J. (2018). Understanding phengite argon closure using single grain fusion age distributions in the Cycladic Blueschist Unit on Syros, Greece. *Earth and Planetary Science Letters*, *484*, 192–203.

Villa, I. M., De Bièvre, P., Holden, N. E., & Renne, P. R. (2015). IUPAC-IUGS recommendation on the half life of 87Rb. *Geochimica et Cosmochimica Acta*, *164*, 382–385.

Wei, C. J., & Clarke, G. L. (2011). Calculated phase equilibria for MORB compositions: a reappraisal of the metamorphic evolution of lawsonite eclogite. *Journal of Metamorphic Geology*, *29*, 939–952.

White, R. W., Powell, R., & Holland, T. J. B. (2007). Progress relating to calculation of partial melting equilibria for metapelites. *Journal of Metamorphic Geology*, *25*, 511–527.

White, R. W., Powell, R., Holland, T. J. B., & Worley, B. A. (2000). The effect of TiO_2 and Fe_2O_3 on metapelitic assemblages at greenschist and amphibolite facies conditions: Mineral equilibria calculations in the system K_2O–FeO–MgO–Al_2O_3–SiO_2–H_2O–TiO_2–Fe_2O_3. *Journal of Metamorphic Geology*, *18*, 497–511.

White, R. W., Powell, R., Holland, T. J. B., Johnson, T. E., & Green, E. C. R. (2014). New mineral activity–composition relations for thermodynamic calculations in metapelitic systems. *Journal of Metamorphic Geology*, *32*, 261–286.

Wijbrans, J. R., & McDougall, I. (1988). Metamorphic evolution of the Attic Cycladic Metamorphic Belt on Naxos (Cyclades, Greece) utilizing 40Ar/39Ar age spectrum measurements. *Journal of Metamorphic Geology*, *6*, 571–594.

Wijbrans, J. R., Schliestedt, M., & York, D. (1990). Single grain argon laser probe dating of phengites from the blueschist to greenschist transition on Sifnos (Cyclades, Greece). *Contributions to Mineralogy and Petrology*, *104*, 582–593.

Young, D. J., & Kylander-Clark, A. R. C. (2015). Does continental crust transform during eclogite facies metamorphism? *Journal of Metamorphic Geology*, *33*, 331–357.

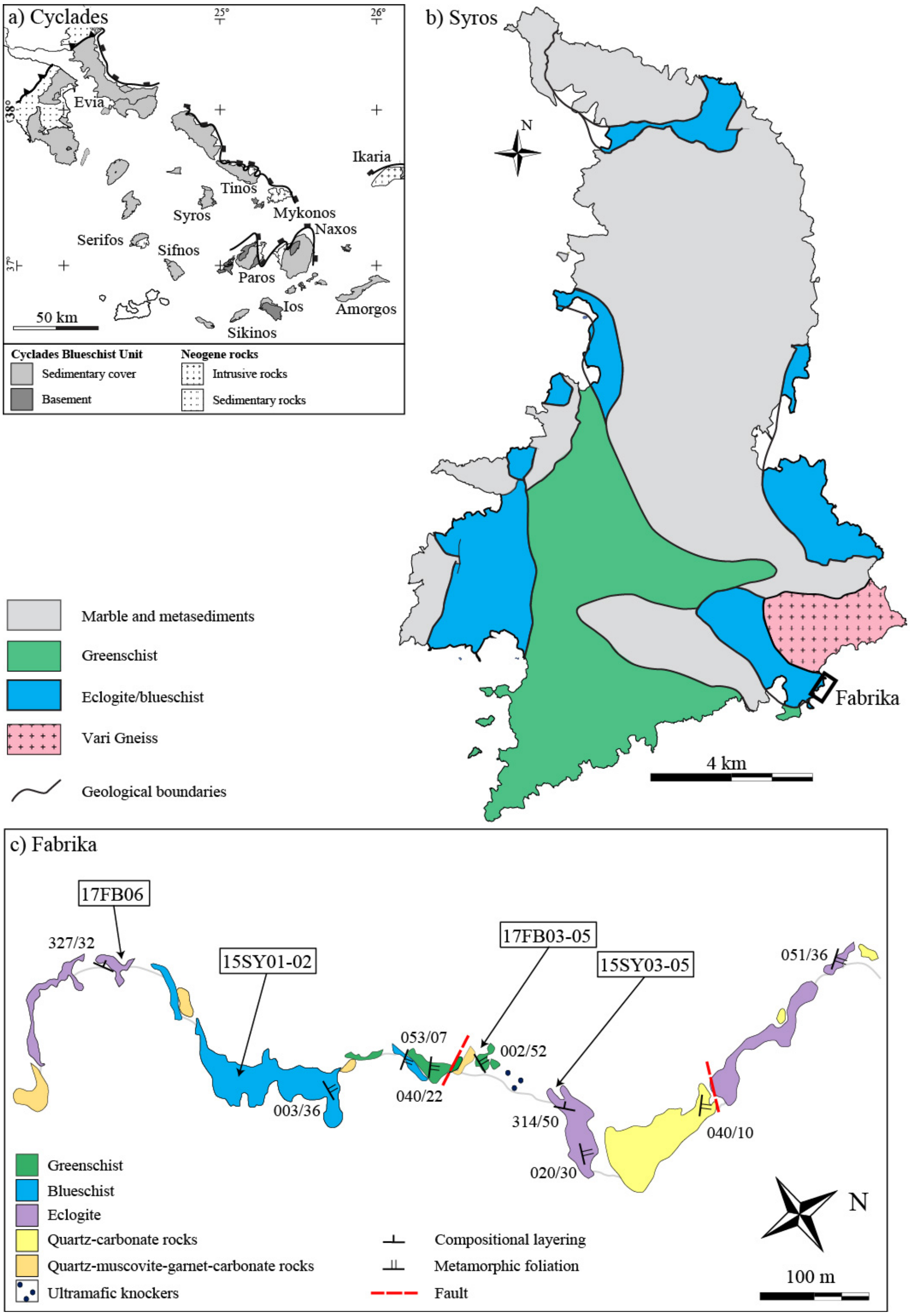

Figure 1: Maps of a) the Cyclades, b) Syros and c) the coastal section and outcrop pattern at Fabrika. Fabrika is located on the map of Syros. The terms “greenschist”, “blueschist” and “eclogite” are used to describe the appearance of rocks in the field not necessarily the corresponding facies. Structural measurements (compositional layering and metamorphic foliation) are shown using the dip direction (3-digits) / dip angle (2 digits) convention. Compositional layering and metamorphic foliations are shown using single and double tick marks, respectively. Faults are shown by red dotted lines.

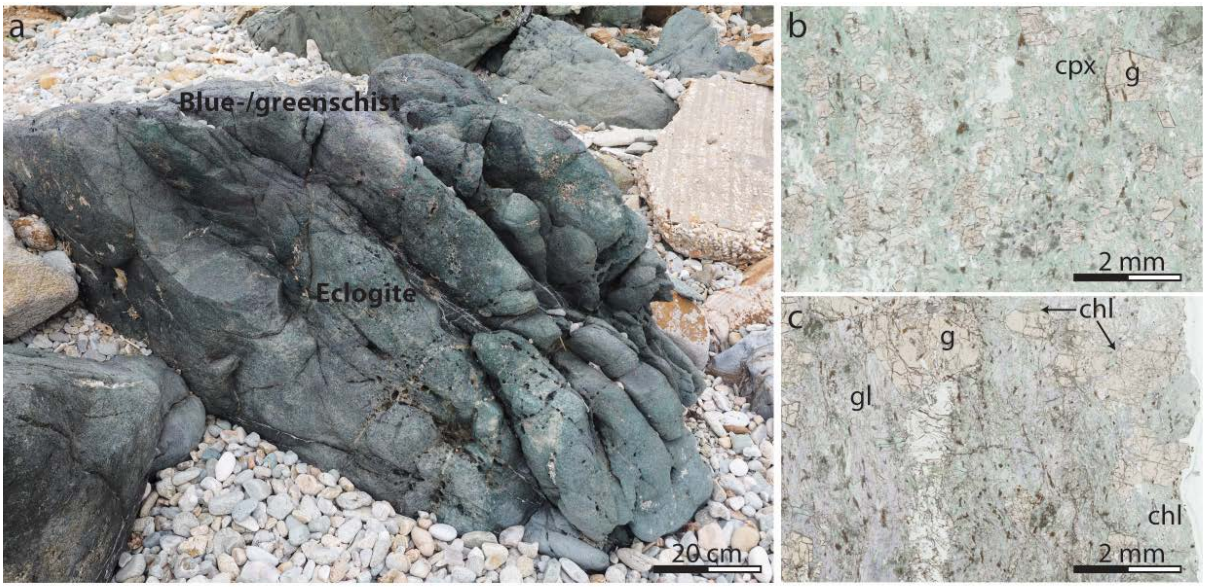

Figure 2: Ultramafic eclogite knocker with a blueschist/greenschist rind: a) field image, and b-c) scanned thin section images in plane polarized showing b) the eclogite facies interior and c) the blueschist/greenschist facies rind of the knocker. Abbreviations used are cpx = clinopyroxene, g = garnet, gl = glaucophane and chl = chlorite.

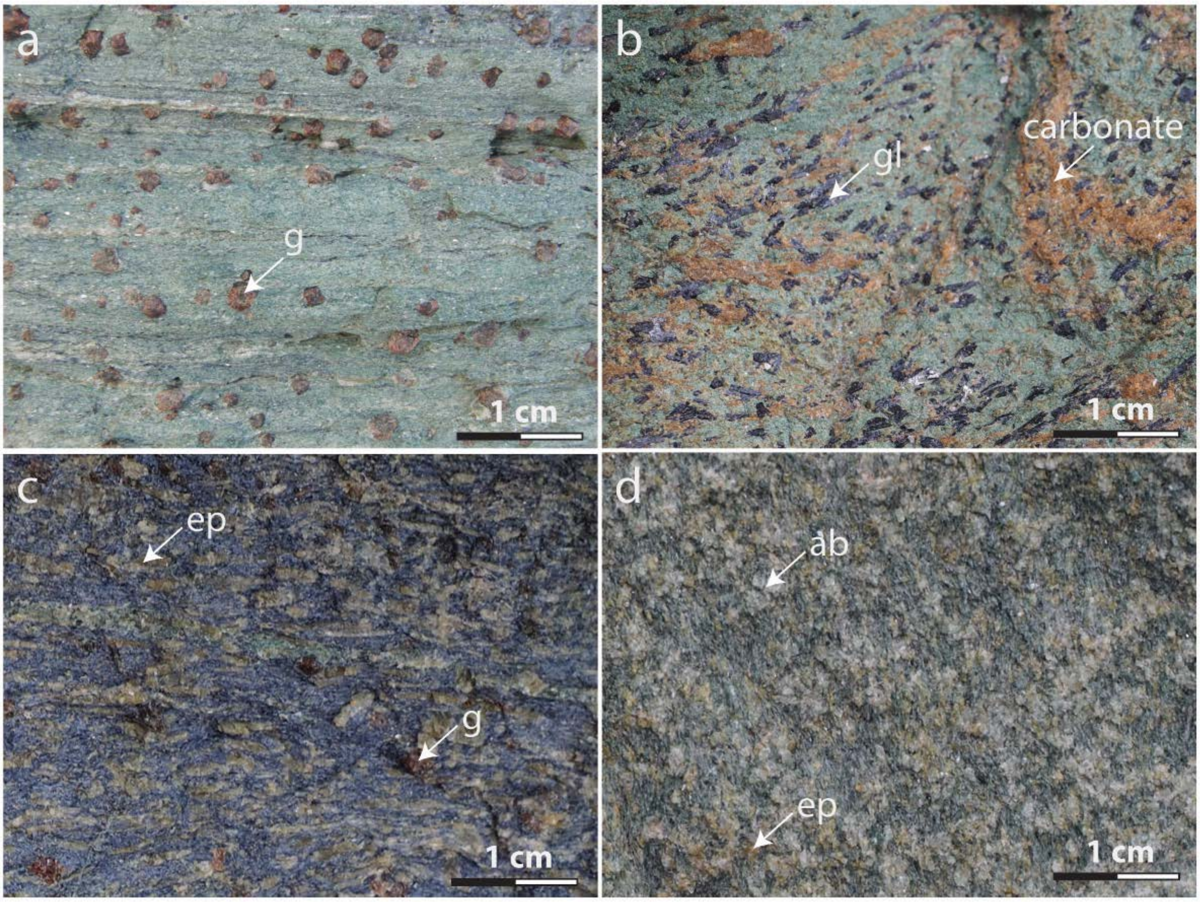

Figure 3: Mafic rocks: a) eclogite with garnets, b) eclogite with glaucophane and carbonate patches, c) blueschist with epidote and garnet, and greenschist with albite and epidote. Abbreviations used are g = garnet, gl = glaucophane, ep = epidote and ab = albite.

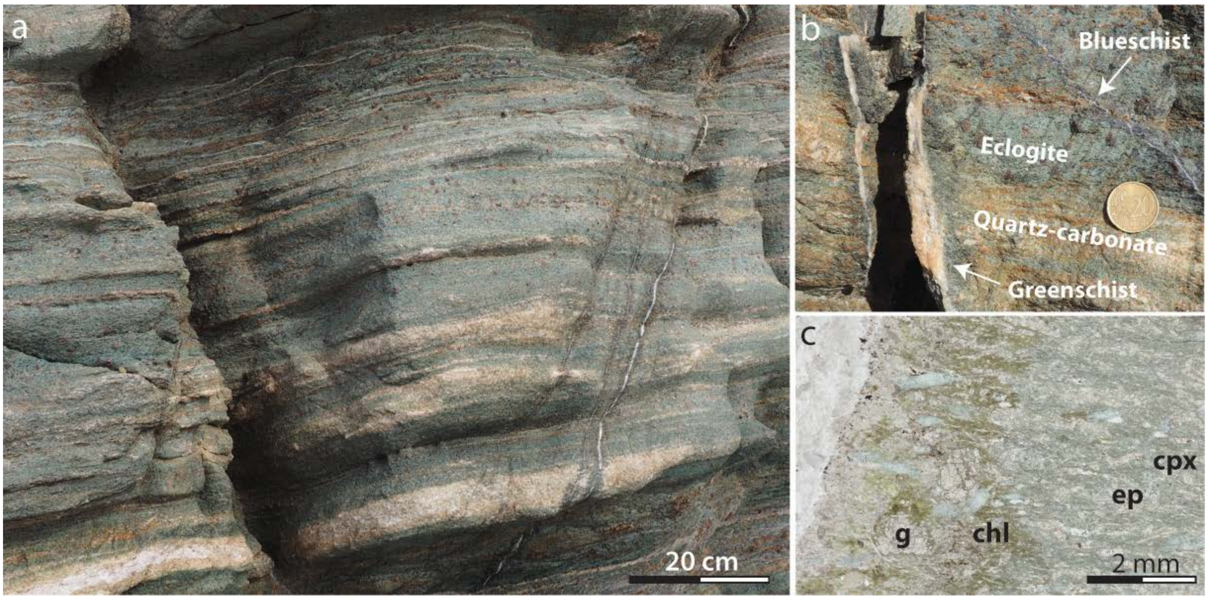

Figure 4: Eclogite: a) field image of layered eclogite (green) and quartz-carbonate rocks (white), b) field image showing replacement of eclogite by blueschist and greenschist alongside quartz-carbonate veins (diameter of coin = 2.2 cm) and c) scanned thin section images in plane polarized showing replacement of eclogite by greenschist facies minerals alongside one of the veins. Abbreviations used are cpx = clinopyroxene, g = garnet, ep = epidote and chl = chlorite.

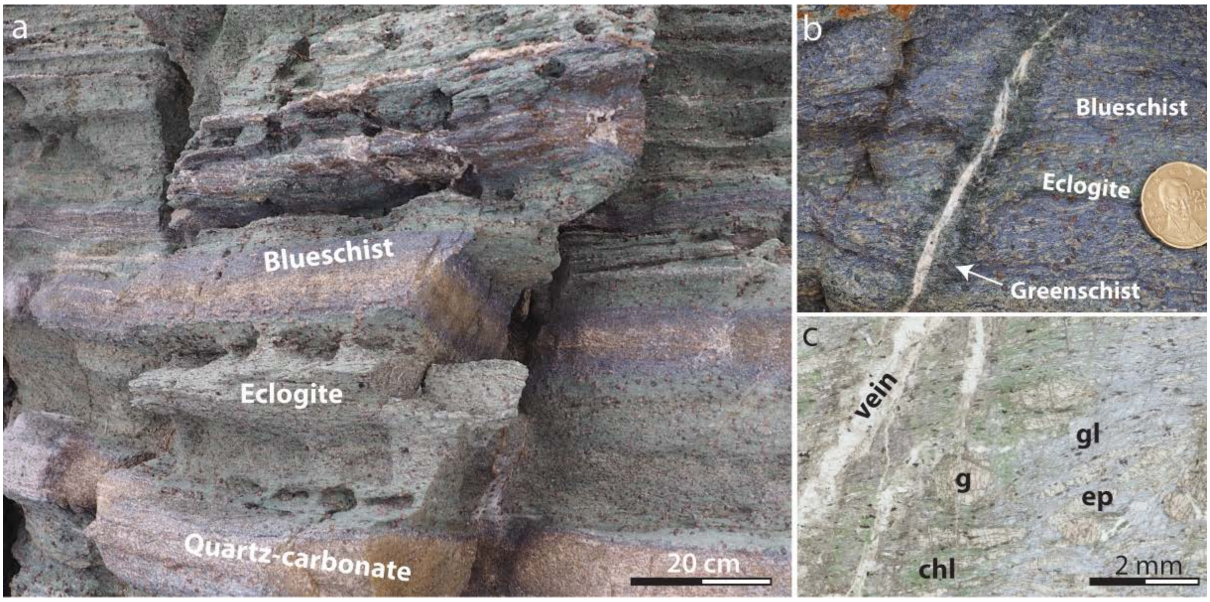

Figure 5: Blueschist: a) field image of layered blueschist, eclogite and quartz-carbonate rocks, b) field image showing replacement of blueschist by greenschist alongside a quartz-carbonate vein (diameter of coin = 2.2 cm) and c) scanned thin section images in plane polarized showing replacement of blueschist by greenschist facies minerals alongside the same vein. Abbreviations used are g = garnet, gl = glaucophane, ep = epidote and chl = chlorite.

Figure 6: Greenschist: field images showing a) massive greenschist and b) replacement of eclogite by greenschist.

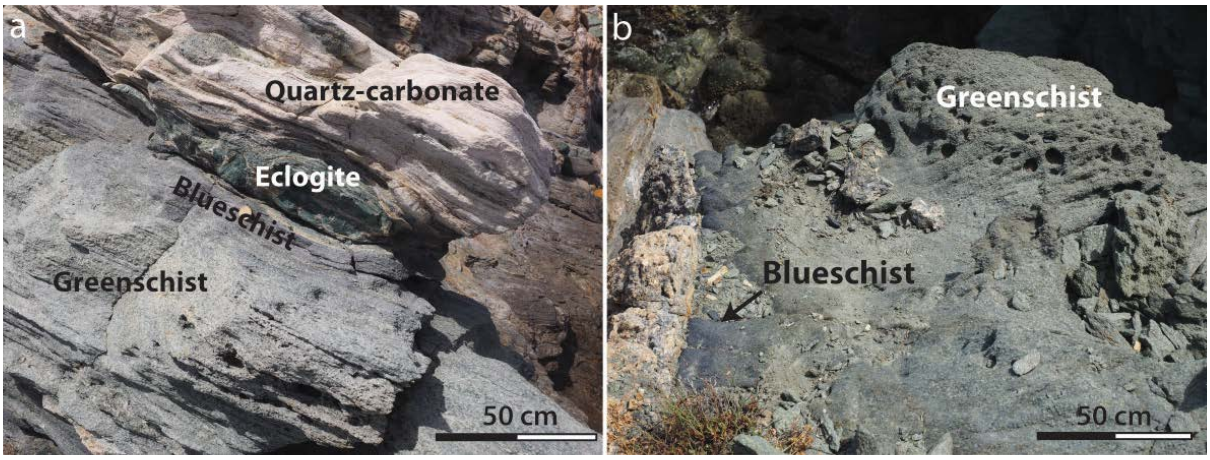

Figure 7: Preservation of a) eclogite and blueschist in greenschist alongside quartz-carbonate layer, and b) blueschist in greenschist alongside a quartz-carbonate vein.

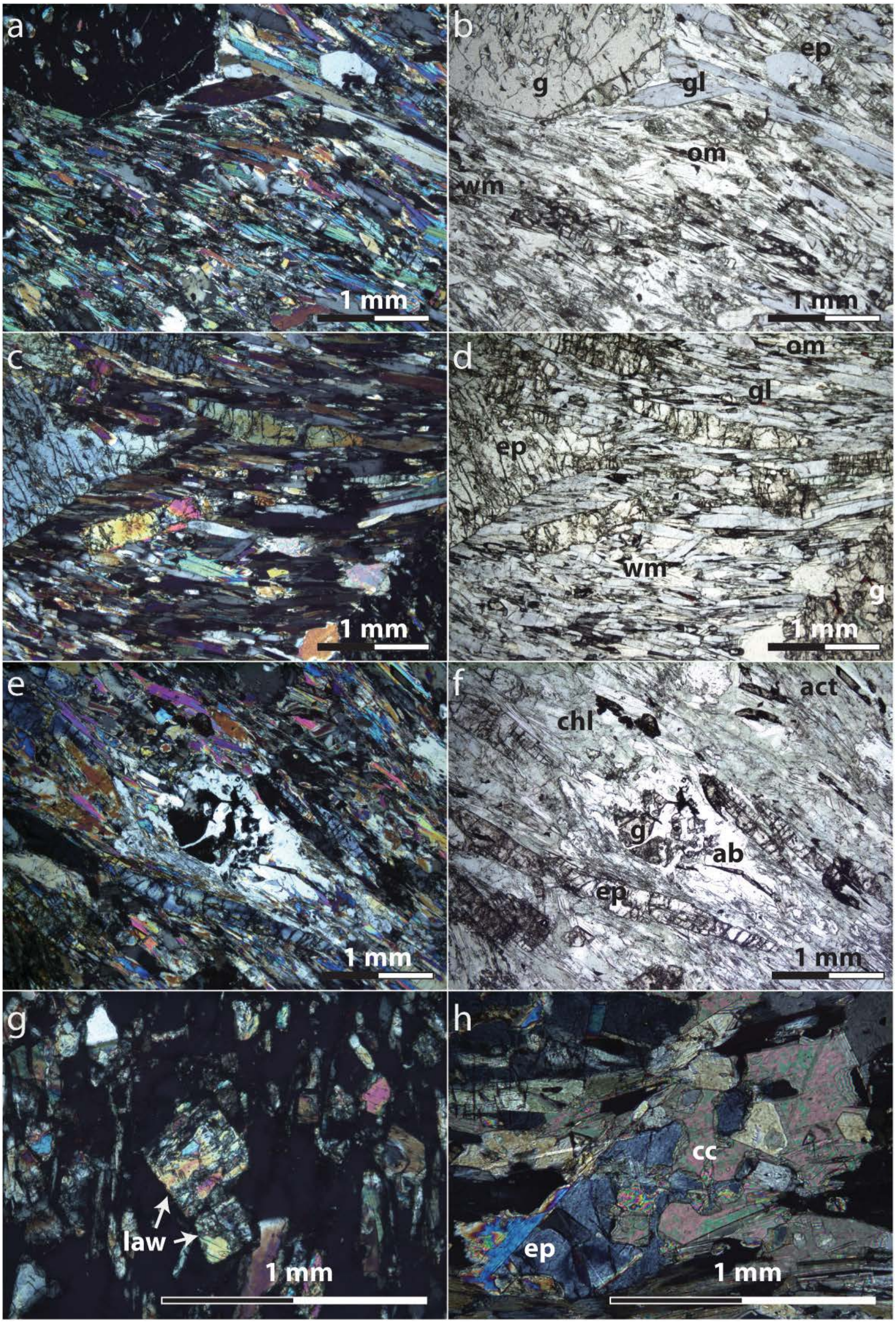
a
1 mm
b
g
gl
ep
om
wm
1 mm
c
1 mm
d
om
gl
ep
wm
g
1 mm
e
1 mm
f
chl
act
g
ab
ep
1 mm
g
law
1 mm
h
cc
ep
1 mm

Figure 8: Photomicrographs of eclogite sample 15SY03 in a) plane-polarised light (PPL) and b) cross-polarised light (XPL), blueschist sample 15SY01 in c) PPL and d) XPL, and greenschist sample 17FB03 in e) PPL and f) XPL, g) lawsonite pseudomorphs included in garnet in sample 15SY01, and h) carbonate replacing epidote in sample 15SY03. Abbreviations used are om = omphacite, gl = glaucophane, act = actinolite, wm = white mica, g = garnet, ep = epidote, law = lawsonite, ab = albite and cc = calcite.

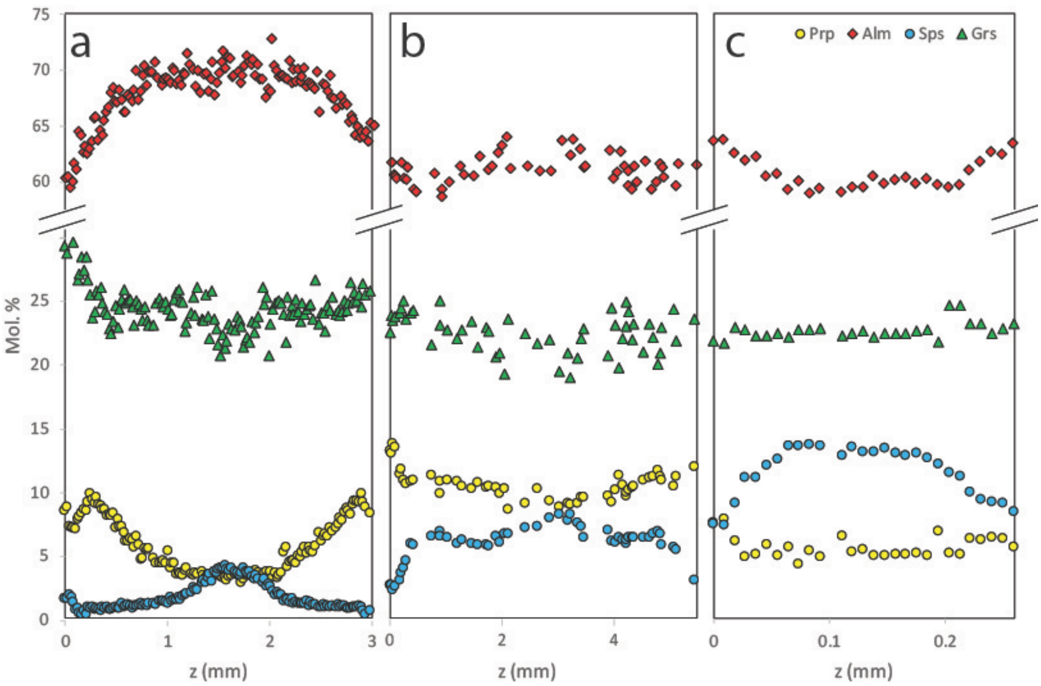

Figure 9: Profiles across garnet porphyroblasts in a) eclogite sample 15SY03 and b) blueschist sample 15SY01 showing weight proportions of almandine (alm), grossular (grs), pyrope (pyr) and spessartine (sps). Garnet cores and inner rims are shaded light grey. Garnet outer rims are shaded dark grey.

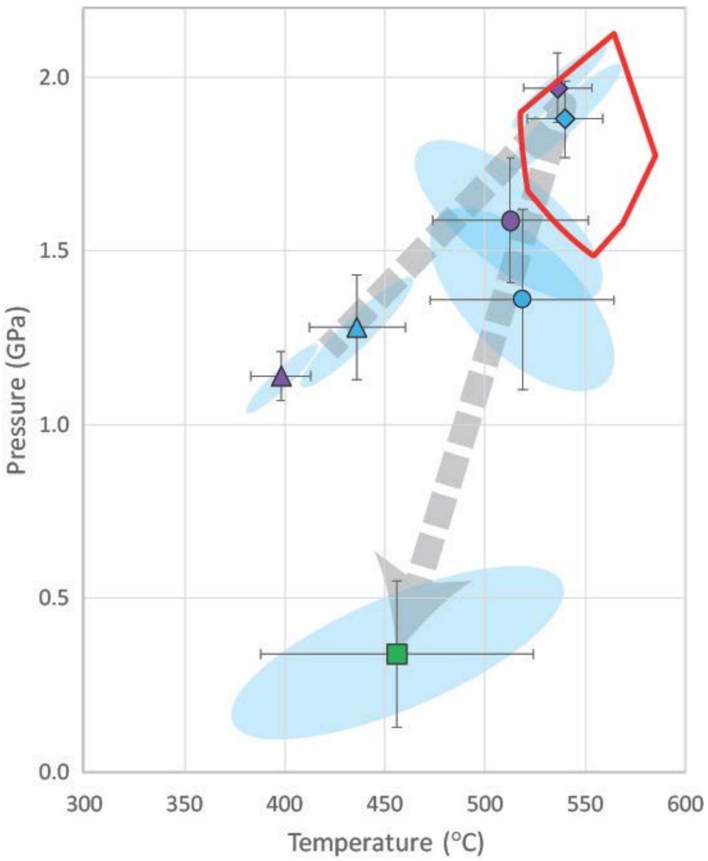

Figure 10: *P-T* diagram showing 1) *P-T* estimates from garnet cores, co-existing inclusions and lawsonite (triangles), garnet inner rims, co-existing inclusions and lawsonite (diamonds), garnet outer rims and matrix minerals (circles) from eclogite sample 15SY03 (purple symbols) and blueschist sample 15SY01 (blue symbols); 2) a *P-T* estimate from greenschist sample 17FB03; 3) a *P-T* estimate for peak metamorphism from the *P-T* pseudosections (Fig. 12); and 4) an inferred *P-T* path (grey dashed line). Error ellipses are based on uncertainty correlations calculated using THERMOCALC.

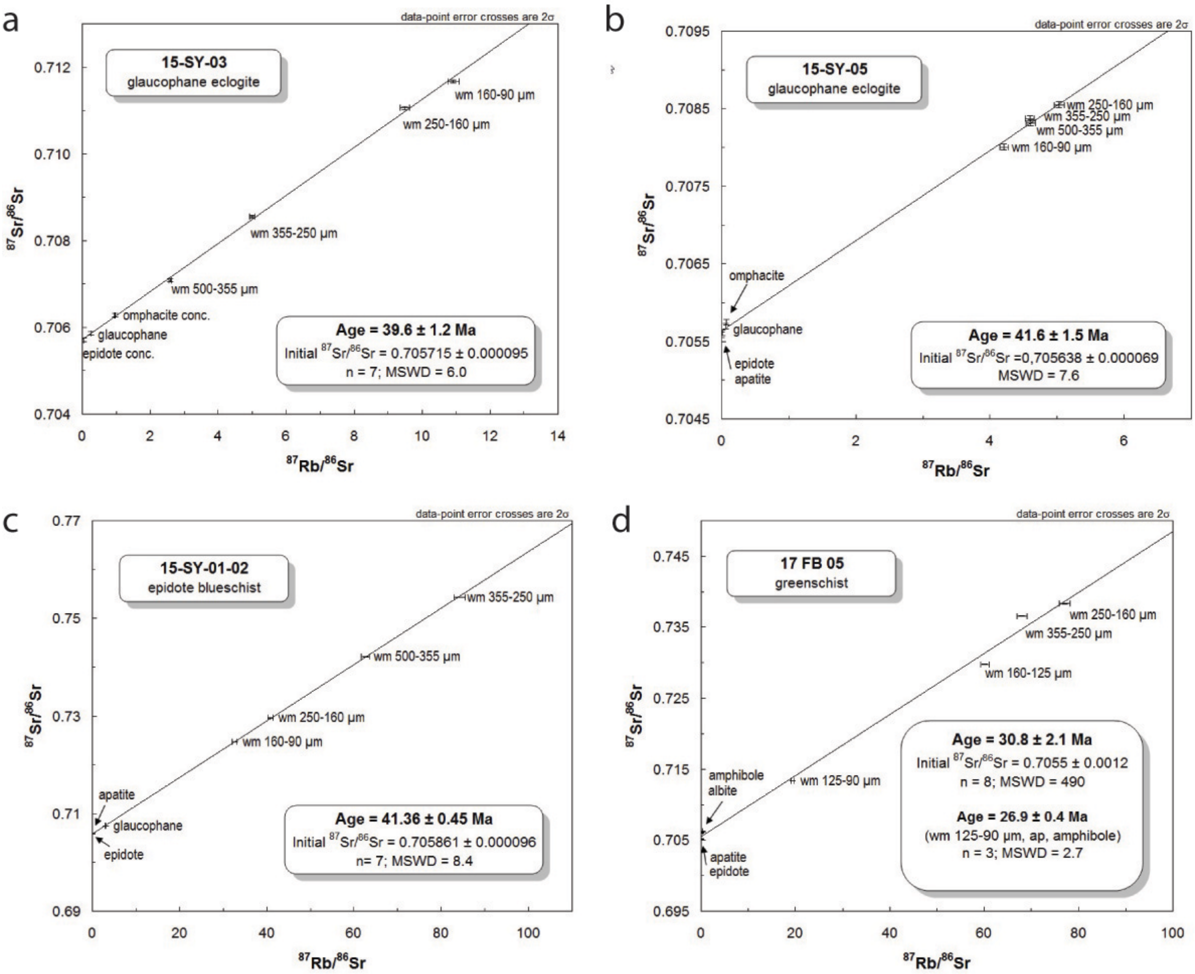

Figure 11: $^{87}Sr/^{86}Sr$ – $^{87}Rb/^{86}Sr$ plots for a) glaucophane eclogite sample 15SY03, b) carbonate-rich glaucophane eclogite 15SY05, c) epidote blueschist 15SY01-02 (parts of both samples) and d) greenschist 17FB05.

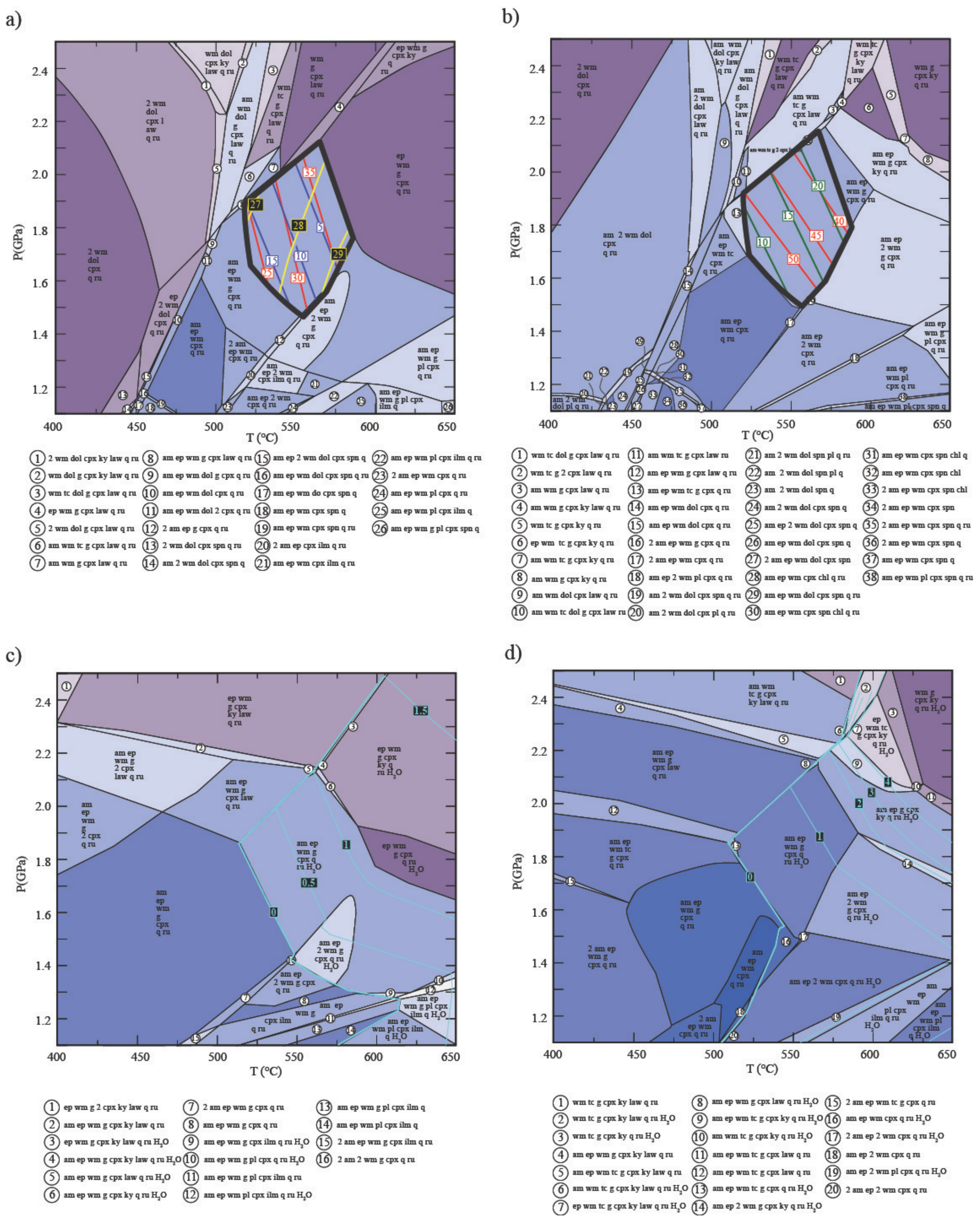

Figure 12: *P-T* pseudosections calculated for the effective rock compositions shown (see methods) for a) eclogite sample 15SY03 and b) blueschist sample 15SY01 at H_2O saturation and for c) eclogite sample 15SY03 and d) blueschist sample 15SY01 with the amount of H_2O defined so that the rock is water saturated at peak metamorphic conditions. Blue-shaded fields contain amphibole, whereas purple-shaded fields do not contain amphibole. The part of the field which contains the observed peak metamorphic assemblage (amphibole

(glaucophane) + clinopyroxene (omphacite) + white mica + garnet + epidote + rutile + quartz) on *both* of pseudosections (a) and (b) is outlined and contoured with modal isopleths for amphibole (red), omphacite (green) and white mica (yellow). Isopleths are not shown for white mica in the blueschist, because the mode is approximately constant (~5 vol. %). Pseudosections (c) and (d) are contoured with modal isopleths for H_2O (blue). Abbreviations used are am = amphibole, cpx = clinopyroxene, wm = white mica, tc = talc, g = garnet, ky = kyanite, sp = spinel, ep = epidote, pl = plagioclase, law = lawsonite, dol = dolomite, cc = calcite, ilm = ilmenite, ru = rutite and q = quartz.